Short Range Order of Hydrocarbon Chains in Fluid Phospholipid Bilayers Studied by X-Ray Diffraction from Highly Oriented Membranes

Alexander Spaar and Tim Salditt
Experimentalphysik, Universität des Saarlandes, Im Stadtwald, D-66123 Saarbrücken, Germany

ABSTRACT We present a study of the short range ordering of hydrocarbon chains in phospholipid bilayers. The x-ray peak associated with the hydrocarbon chains has been probed by means of reciprocal space mappings. Using 20 keV undulator radiation and samples of negligible mosaicity (orientational disorder), the intensity distribution is probed as a function of two coordinates, the momentum transfer parallel and perpendicular to the bilayer, over a wide range and at high resolution. Structural results are obtained concerning the distribution of tilted segments, the correlation length and the radial distribution function of the quasi two-dimensional liquid structure. A comparison is made with published molecular dynamics data (H. Heller, M. Schaefer, and K. Schulten. 1993. *J. Phys. Chem.* 97:8343–8360) by direct Fourier transformation of the atomic coordinates. The exact prefactor in the relationship between interchain distance and peak position is derived.

INTRODUCTION

The structure of lipid membranes in the liquid L_α phase is an important basis of membrane biophysics. Early studies of x-ray and neutron scattering have already attributed the relatively broad intensity maximum observed around 1.4 Å^{-1} to the short range order of the fluid acyl chains (Warren, 1933; Luzzati, 1968; Levine and Wilkins, 1971). Usually, just two parameters are derived from the peak: a mean interchain distance a and a correlation length ξ of the decaying positional correlations. Contrarily, the diffraction pattern of more ordered bilayer phases encountered at lower temperatures and hydration gives access to many more structural parameters. Lattice symmetry, lattice constants, lattice angles, and chain tilt angles and directions, as well as an eventual ripple periodicity and amplitude, can all be determined (Smith et al., 1988; Sun et al., 1994; Katsaras, 1995). At the same time it is clear that a liquid phase cannot be structurally defined only by two parameters. Although the angular information on the liquid coordination and short range order is lost due to the phase problem, the radial distribution function $g(r)$ is typically well known for simple liquids. An oriented and highly correlated phase of hydrocarbon chains in the fluid bilayer is a more complex issue. To this end, NMR resonance techniques using single site deuterium labels have provided a way to measure an order parameter profile of the fluid chains (Seelig and Seelig, 1977, 1980), quantifying the increasing disorder of the chains toward the center of the bilayer (see Fig. 1 *a*). Thermodynamic mean field models have also been developed to describe the chain organization in bilayers (Ben-Shaul et al., 1985).

More recently, new computational tools have been used to study the structure and dynamics of lipid bilayers by molecular dynamics (MD) simulations. As we show below, the simultaneous use of MD and diffraction data can lead to refined structural models of lipid bilayer systems. The simulation can help to interpret diffraction signals with more detail and accuracy than it was possible before. At the same time, starting parameters and interatomic potentials used in MD can be verified and refined by comparison with diffraction data. A direct comparison can be made by means of a Fourier transform of the MD coordinates.

In this article we present x-ray experiments on the structure of the fluid L_α phase in three well-known phospholipid model systems: 1,2-dilauroyl-*sn*-glycero-3-phosphatidylcholine (DLPC), 1,2-dimyristoyl-*sn*-glycero-3-phosphatidylcholine (DMPC), and 1-oleoyl-2-palmitoyl-*sn*-glycero-3-phosphatidylcholine (OPPC). The data have been collected on highly aligned multilamellar samples deposited on Silicon substrates, using the scattering geometry of grazing incidence diffraction (GID). Highly brilliant undulator radiation in combination with a two-dimensional (2D) x-ray CCD camera yields well-resolved reciprocal space mappings (RSM) over a large range in momentum transfer, both parallel q_0 and perpendicular q_z to the plane of the bilayer. At the same time the acquisition times are small enough to prevent radiation damage. RSMs have been used also to study the interaction with antimicrobial peptides (Yang et al., 1999; Münster et al., 2002) and membrane proteins (Müller et al., 2000). Here we concentrate on the most prominent feature in the RSM, the acyl chain correlation peak, also called paraffin peak in the literature. This peak or maximum is attributed to the short range ordering of the fluid chains. Correspondingly, it can also be called the structure factor $S(q_0, q_z)$ of the L_α phase. The peak intensity is distributed over a circle with radius around $q_0 = 1.4$ Å^{-1}, with a maximum at $q_z = 0$ Å^{-1}. (Refraction effects can lead to a small shift away from the $q_z = 0$ axis, depending on the critical angle α_c. For the silicon

Submitted August 21, 2002, and accepted for publication March 6, 2003.

Address reprint requests to Alexander Spaar, E-mail: a.spaar@mx.uni-saarland.de; or to Tim Salditt, E-mail: tsalditt@gwdg.de.

Tim Salditt's present address is Institut für Röntgenphysik, Geiststr. 11, Universität Göttingen, D-37073 Göttingen, Germany.

0006-3495/03/09/1576/09 $2.00

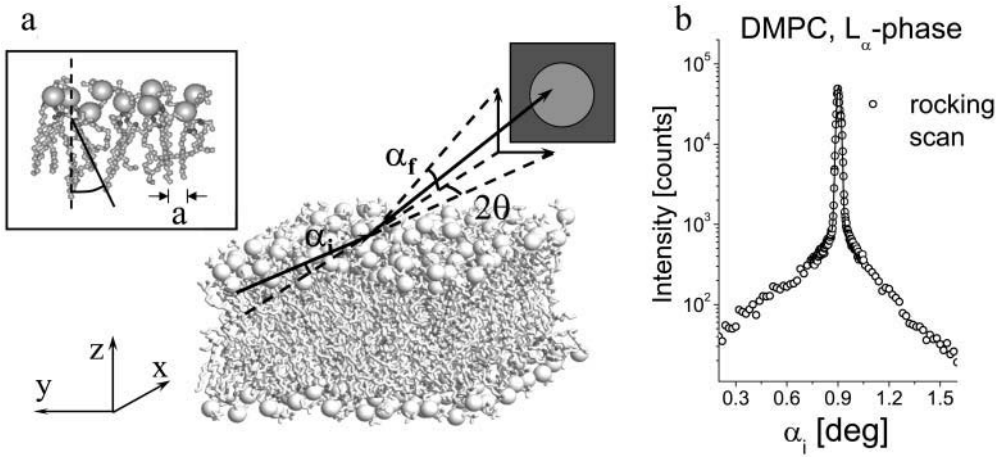

FIGURE 1 (*a*) Sketch combining the MD data set (Heller et al., 1993) and the scattering geometry used. The phosphorus atoms have been enlarged to mark the lipid headgroups. The momentum transfer vertical to the membrane plane q_z is controlled by the scattering angle $\alpha_i + \alpha_f$, the lateral momentum transfer $q_\parallel$ mainly by 2θ. The insert illustrates the mean interchain distance a and the tilt angle. (*b*) Rocking curve of DMPC in the L_α phase (on logarithmic scale) evidencing the high degree of orientation.

substrate at 20 keV, we have $\alpha_c = 0.089°$.) It is important to note that the intrinsic intensity distribution can be measured only from samples with highly oriented lamellar domains, unaffected by smearing due to mosaicity. In the present case, the width of the angular distribution of bilayer normal vectors (mosaicity) was below 0.02° halfwidth at half maximum (HWHM).

Two main problems are addressed:

a. How can the peak position q_0 and width ω be quantitatively correlated to the real-space structure of the lipid acyl chains? In a naive approach, the interchain distance a in between the chains would be calculated from the peak position according to $a = 2\pi/q_0$. To be more precise, we define a as the most likely interchain distance, i.e., as the first maximum of the pair-pair correlation function $g(r)$. It has to be distinguished from the mean interchain distance $a_m = \int_{1sh} rg(r)dr / \int_{1sh} g(r)dr$, where $\int_{1sh}$ denotes the integration over the first shell, i.e., up to the first minimum in $g(r)$. It is already clear from estimations of the average area per lipid headgroup $2\,A_L$ (i.e., per two acyl chains) that a must be larger than $2\pi/q_0$. A_L can be inferred from the bilayer density profile, as obtained by sophisticated liquid crystallography methods developed in recent years (Nagle and Wiener, 1988; Wiener and White, 1992; White and Hristova, 2000; Nagle and Tristram-Nagle, 2000). Here we derive the prefactor c in the relation $a = c/q_0$. Of course, it is well known already from simple liquids that $c = 2\pi$ generally does not hold.
b. The second problem is related to the correlation length ξ associated with the width ω of the peak, and more generally, to the form of the pair-pair correlation function (radial distribution function) $g(r)$ of the chains in the bilayer.

Note, that problem (a) is posed and treated in the framework of a 2D liquid. This is justified, since a must be constant for all xy cross sections through the chains of a planar bilayer, independent of z. Moreover, the MD data show that these 2D cross sections are characterized not only by the same a but also by the same radial distribution function $g(r)$, despite the fact that the statistics of chain tilt angles may change with z. Finally, a horizontal cut through the RSM $S(q_z = 0, q_\parallel)$ measures the lateral correlations after vertical averaging over the chain, or equivalently the 2D correlations of the center of mass coordinates projected onto the xy plane.

While problem (a) thus addresses the statistical properties in 2D space, the second problem concerns the distribution of the correlated acyl chains in 3D space. It can be posed by way of the following questions: (b) How can the tilt angles and the distribution of chain tilt angles be determined from the RSM, in particular the decay of the scattering intensity with the polar angle ϕ on the circle in reciprocal space? How can the observed broadening of the peak, i.e., the curve $\omega(\phi)$, be interpreted?

To answer these questions we use the RSM data, in combination with a published study of MD simulations carried out on a bilayer of 200 1-palmitoyl-2-oleoyl-*sn*-glycero-3-phosphatidylcholine (POPC) molecules in the L_α phase (Heller et al., 1993). Note that since this seminal study, many more simulations, also on longer timescales, have been performed on various lipid membrane segments (Feller 2000; Koubi et al., 2000; Lindahl and Edholm, 2000; Mashl et al., 2001; Tieleman and Berendsen, 1996). However, unfortunately not all coordinates are freely accessible or deposited on a data bank. On these coordinates we apply various statistical evaluation schemes and Fourier transforms for comparison with the experiment. At the same time, analytical Fourier transforms of the measured structure factor $S(q_\parallel)$ with and without simplifying approximations are directly compared to the MD data. As a result, the radial distribution function $g(r)$ can be derived, from which we determine $a = 9\pi/(4q_0)$.

MATERIALS AND METHODS

The lipids DLPC, DMPC, and OPPC were purchased from Avanti Polar Lipids (Birmingham, AL) with a purity of >99%, and used without further

purification. Although experiments were carried out on OPPC, POPC molecules were used in the MD simulation (Heller et al., 1993). However, we think that the interchange of the two acyl chains positions is of minor importance for the short range order in the hydrocarbon layer that is of interest in this study, so that a reasonable comparison between experiment and simulation can be made. The lipids were first dissolved in isopropanol at a concentration of 20 mg/ml, and spread onto silicon substrates ((111)-orientation, 1-inch diameter), following essentially the procedure described by Seul and Sammon (1990). The wafers were cleaned by subsequent washing in methanol, and made hydrophilic in a plasma cleaner for about half a minute. Between each step, the wafers were thoroughly rinsed with ultrapure water (specific resistance $\geq$18 MΩ cm, Millipore, Bedford, MA). A drop of 0.2 ml was then carefully spread onto the substrate, which was placed on a spin coater. The angular velocity was chosen to 230 rpm, fast enough for aligning the membranes, preventing film rupture and dewetting, but also slow enough to keep the whole solvent on the wafer (Mennicke and Salditt, 2002). After 10 min, the sample was dried, yielding a very uniform film. Remaining traces of solvent in the sample were removed by exposing the samples to high vacuum over 24 h. The films were then rehydrated in a hydration chamber. The orientational alignment of the multilamellar stack with respect to the substrate (mosaicity) was typically better than 0.02° (HWHM, see Fig. 1 *b*). A very low mosaicity is a prerequisite to apply interface-sensitive x-ray scattering techniques for structural studies of solid-supported bilayers.

Sample environment

During the x-ray experiments, the solid-supported multilamellar films were kept in a closed temperature-controlled chamber. The chamber consists of two concentric aluminum cylinders, with Kapton windows. The inner cylinder was kept at a constant temperature of $T = 45$°C by a flow of oil, connected to a temperature-controlled reservoir (Julabo, Seelbach, Germany) with PID control. The space between the two cylinders was evacuated to minimize heat conduction. The temperature was measured close to the sample holder by a Pt100 sensor, indicating a thermal stability of better than 0.02 K over several hours. At the bottom of the inner cylinder, a water reservoir was filled with salt-free Millipore water, such that the sample was effectively facing a vapor phase of nominally 100% relative humidity. Despite the nominally full hydration condition, the DMPC bilayers were typically swollen up to a repeat distance of only $d \simeq 50$ Å in the fluid L_α phase, i.e., they were only partially hydrated. This limited swelling of solid-supported lipid films is well known as the so-called vapor-pressure paradox (Podgornik and Parsegian, 1997), and can only be circumvented in chambers of special design (Nagle and Katsaras, 1999).

X-ray experiment

The samples were characterized by x-ray reflectivity at the experimental station D4 (bending magnet) of the synchrotron radiation source at HASYLAB/DESY (Hamburg, Germany) using photon energy of 20 keV. The grazing incidence (GID) experiments have been carried out at the undulator beamline ID1 of the European Synchrotron Radiation Facility (Grenoble, France) at the same photon energy, as defined by a double bounce Si(111) monochromator. Compared to smaller energies $E < 20$ keV, the ratio of the scattering cross section to the photoabsorption cross section is significantly higher at 20 keV, so that radiation damage is minimized. While the undulator performs well also at $E > 20$ keV, the CCD detector sensitivity is expected to decrease strongly with E. The scattering intensity was recorded by a Princeton CCD camera with a resolution of 1242 $\times$ 1152 pixels, mounted on the detector arm of the ID1 six-circle diffractometer. The pixel positions on the camera correspond to diffraction angles $\alpha = \alpha_i + \alpha_f$ (in the plane of incidence) and 2θ (out of the plane of incidence, see Fig. 1 *a*). From these angles, the different components of the wave vector (momentum transfer) can be calculated as

$$q_x = \frac{2\pi}{\lambda}(\cos\alpha_f \cos(2\theta) - \cos\alpha_i), \quad q_y = \frac{2\pi}{\lambda}\cos\alpha_f \sin(2\theta),$$
$$q_z = \frac{2\pi}{\lambda}(\sin\alpha_i + \sin\alpha_f).$$

A wide range of reciprocal space was then mapped by moving the camera to well-chosen positions, taking a set of five exposures with partial overlap, each with an acquisition time of 100 s and 300 s. By combining these five exposures, we got an image of the reciprocal space (for example, see Fig. 2). The direct beam was blocked by lead tape at the side of the camera. The angle of incidence was chosen to optimize scattering volume, and to minimize background from the substrate (penetration depth). At the same time, a strong specular reflection has to be avoided. For the example given in Fig. 2, the incidence angle was $\alpha_i = 0.5°$ for all exposures, except for the one in the forward direction showing the strong diffuse Bragg sheets, which has been measured at $\alpha_i = 1°$ to avoid detector saturation. At these small angles, the momentum transfer in the direction of the primary beam q_x is always dominated by q_y, even at high q_z, except for very small q_y around the incidence plane, which are not considered here. Therefore it is an excellent approximation to set $q_{\|} = \sqrt{q_x^2+q_y^2} \simeq q_y$ for almost the total range of the RSM (Salditt et al., 1995), in particular in the vicinity of the chain correlation peak. In this approximation, the vertical and parallel components of the momentum transfer are orthogonal.

The setup and more experimental details will be given somewhere else (Salditt et al., unpublished), along with a discussion of the optimum photon energy and the choice of detector (2D CCD versus scintillation counter with two-slit collimation). Importantly, a beam flux at the sample on the order of 10^{11} photons per second as obtained by vertical and horizontal focusing at ID1 led to radiation-induced shifts in the diffraction intensity after ~60 min, a time that is too short for the positioning of a point detector during a 2D mesh scan. Contrarily, the use of the CCD cut down the acquisition time below the threshold for observable radiation damage. The absence of radiation damage has been cross-checked by translating the sample through the beam, sized 0.5 mm (horizontal) $\times$ 0.2 mm (vertical).

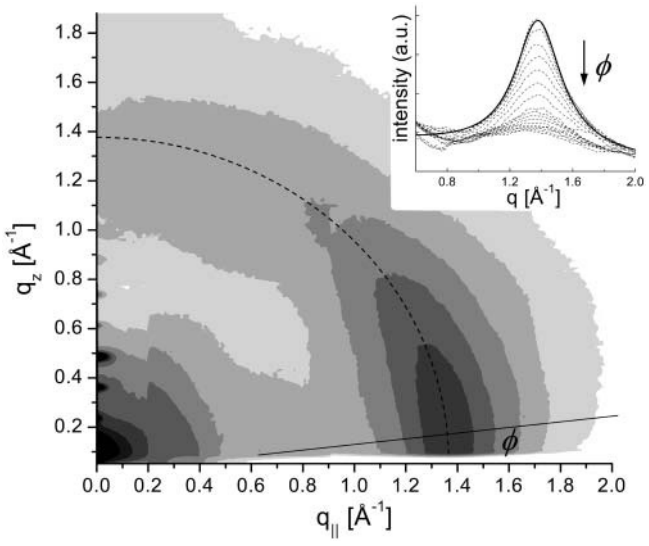

FIGURE 2 Reciprocal space mapping of pure OPPC in the fluid L_α phase. The chain correlation peak is extended along a circle with the radius of $q \simeq 1.38$ Å^{-1}. The inset shows a set of radial slices (*dashed curves*) at different angles ϕ, ranging from $\phi = 5°$ (largest peak) to $\phi = 90°$ (lowest peak). The solid line represents a least-square fit of the 10° slice to a Lorentzian.

RESULTS

The lateral structure of the membranes on molecular length scales can be probed by measurements taken in the GID mode (see illustrating sketch in Fig. 1 *a*). This interface-sensitive scattering method has evolved over the last two decades as a powerful tool in surface and subsurface analysis of crystalline solids (Dosch, 1992). The x-ray optics and refraction effects are used to efficiently discriminate against bulk background signal and to gain depth resolution. Here we apply the method to a highly oriented stack of lipid membranes to study the lateral ordering of acyl chains. Compared to diffraction studies of monolayers (Helm et al., 1987), highly aligned multilamellar membranes offer the advantage of much higher signals and allow the study of complete bilayer systems. The high degree of orientational order is evidenced by rocking scans, see, e.g., the rocking scan around the position of the first Bragg sheet shown in Fig. 1 *b* for DMPC in the L_α phase, measured at an in-house rotating anode with CuK_α radiation. The central width of 0.017° (HWHM) is close to the resolution of the instrument. On logarithmic scale, broad tails are observed two orders of magnitude below the central maximum. Note that these wings do not correspond to disordered domains, but to coherent diffuse scattering stemming from thermal fluctuations (Salditt et al., 1999). The distinction between both cases can be made unambiguously by inspection of the scattering pattern at very small angles around the Bragg peak on the CCD. Whereas incoherent superposition of unoriented domains leads to a circular arc, the coherent diffuse scattering manifests itself in the form of a straight streak on the two-dimensional CCD, or equivalently in three-dimensional reciprocal space as a planar sheet at constant $q_z = 2\pi/d$.

The scattering cross section as probed in grazing incidence diffraction can be written in distorted-wave Born approximation as (Dosch, 1992)

$$\frac{d\sigma}{d\Omega} \propto |T_i(\alpha_i)T_f(\alpha_f)|^2 S(q_\parallel, q_z), \quad (1)$$

where $T_{i/f}$ denote the Fresnel transmission functions that lead to the characteristic Vineyard peaks when α_i or α_f equals the critical angle α_c. In contrast to these optical effects, the structural information is contained in the structure factor

$$S(q_\parallel, q_z) = \left\langle \left| \int d\mathbf{r}\, \rho(\mathbf{r}) e^{i\mathbf{qr}} \right|^2 \right\rangle, \quad (2)$$

where the vertical scattering depth along z can be tuned by α_i and α_f.

In aligned bilayers, the electron density $\rho(\mathbf{r})$ is isotropic in the x-y plane. The reciprocal space needed to describe the system is therefore essentially 2D defined by the vertical q_z and lateral $q_\parallel$ axis, respectively. Particular Fourier components of $\rho(\mathbf{r})$ can be sampled depending on the area of q_z-$q_\parallel$ space that is probed.

Fig. 2 shows the RSM of pure OPPC in the fluid L_α phase, represented in logarithmic gray shades. The upper right corner of the RSM is white since this region has not been mapped. The area below $q_z = 0.09$ Å^{-1} is shadowed by the sample horizon. The lamellar structure leads to pronounced diffuse Bragg sheets in the small **q** region (the primary beam is located below the image). From the peak positions, the lamellar periodicity $d = 50.2$ Å can be determined. Here we focus on the chain correlation peak, which is stretched along a circle with radius $q = \sqrt{q_o^2 + q_z^2} \simeq 1.38$ Å^{-1} (the periodicity in DMPC was $d = 47.7$ Å and in DLPC $d = 43.2$ Å, the peak was located at $q = 1.40$ Å^{-1}, and $q = 1.39$ Å, respectively). An oblique cut through the peak at a given angle ϕ to the sample horizon shows a Lorentzian lineshape. This result has been verified in many different experiments. It was recognized that the peak position is a function of temperature, humidity, lipid type, etc. The peak can be attributed to correlated chains with different tilt angles with respect to the membrane normal. The peak parameters, maximum peak intensity, or alternatively the integrated intensity (i.e., area beneath the peak), as well as the peak width (HWHM) ω can be evaluated as a function of ϕ for the corresponding cuts through the 2D intensity matrix of the RSM. To this end, least-square fits using Lorentzian lineshapes with linear background have been employed. Over the range of the peak, the assumption of a linear background was judged to be sufficient, in particular since the linear slopes were generally quite small. Furthermore, dark current and detector sensitivity measurements show a flat behavior. Strong nonlinearities are observed in the background close to the specular and primary beam, but are far away from the chain correlation peak. In the following, we analyze the data to get information about the flexibility of the chains, the ratio of tilted chains. and the interchain distance of $a \simeq 4.9$ Å.

In the inset of Fig. 2, radial slices (*dashed curves*) for different angles ϕ are displayed, ranging from $\phi = 5°$ (*top curve*) to $\phi = 90°$ (*bottom curve*). The lineshape of the peak is Lorentzian as can be seen from the least-squares fit, e.g., of the 10° slice (*solid line*). The data show a systematic decrease of the peak maximum, accompanied by an increase of its width. The fitting results for the area $A(\phi)$ and the correlation length $\xi(\phi) = 1/\omega(\phi)$ of the background subtracted peak are displayed in Fig. 3. Without liquid structure models or molecular coordinates at hand, this behavior has been tentatively interpreted as follows (Salditt, 2000): The intensity scattered into the direction of ϕ is attributed to a population of chain segments tilted at an angle ϕ with respect to the bilayer normal. It is therefore a measure of the angular distribution of the chains. The constant peak position indicates that tilted chains (or chain segments) are characterized by the same mean interchain distance. The increasing width $\omega(\phi)$ reflects the decreasing correlation length $\xi(\phi)$ of the tilted segments. With this interpretation, the distribution of tilt angles ϕ can be determined by the integrated intensities. However, the present interpretation in the form

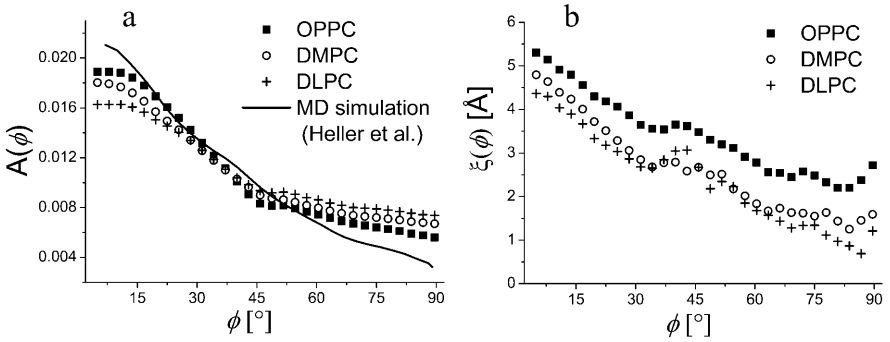

FIGURE 3 (*a*) Integrated intensity of the background-subtracted chain correlated peak for the lipids OPPC, DMPC, and DLPC for various angles ϕ normalized to the integral of the curve (see Table 1). These curves can be interpreted as a distribution of the chains with respect to the angle between the projection of the chains to the *y-z* plane and the membrane normal. For comparison, the calculated distribution of the lipid chains from the MD data set with respect to the same angle is shown. (*b*) Correlation length as a function of ϕ is obtained from the peak width $\omega(\phi)$ (HWHM) as $\xi(\phi) = 1/\omega(\phi)$. The graphs behave inversely to $A(\phi)$: Long lipid chains are better correlated than short ones and vice versa.

of populations of tilted segments must be regarded with caution. A better description could be made in the future by modeling the 2D intensity distribution on the basis of a mean-field model (Ben-Shaul, 1985) or other theories of the complex liquid structure of lipid chains. Alternatively, we follow an approach, where the atomic coordinates of MD simulation are Fourier transformed and compared to the measured 2D intensity distribution, as shown below.

Fig. 3 shows (*a*) the integrated peak intensity and (*b*) the correlation length as a function of ϕ for the lipids OPPC, DMPC, and DLPC. The integrated intensities $A(\phi)$ are therefore normalized to the area under the curves $\int A(\phi)d\phi = 1$. The angle ϕ corresponds to the angle between the bilayer normal (*z* axis) and the projection of the chain to the *y-z* plane, rather than the angle between the chain and bilayer normal. For comparison, we have calculated the angular chain distribution from the MD data set (*solid line* in *a*), also with respect to the angle between the projected chains and the bilayer normal. This curve has also been normalized to its integral (i.e., the area under the curve), so that there is no free adjustment parameter. The simulation agrees qualitatively but not quantitatively with the experimental curves. The reason for this is probably due to the fact that the interpretation of $A(\phi)$ in terms of the angular distribution is too simplistic, since the scattering intensity at a given position on the detector is the sum over contributions of chains with different tilt angles, or a range of tilt angles. Furthermore, this sum must not necessarily be an incoherent sum of the intensities. Therefore, we model the peak by a Fourier transform of the real space coordinates below. At this point we compare the different experimental curves empirically and quantitatively. The plots of $A(\phi)$ show a similar behavior for the three lipids; the decrease is an indication for the different flexibility of the chains in the membranes. DLPC has short tails (12:12); they are therefore very flexible and thus there is a greater fraction of chains with a larger tilt angle than in DMPC (14:14) and OPPC (16:18). Contrarily, the long tails of OPPC are relatively stiff compared to DMPC and DLPC; correspondingly more than half of the scattered intensity is found at angles $\phi \leq 30°$. The exact values of the fractions of $A(\phi)$ between 0° and 30°, respectively 60° and 90°, are listed in Table 1. The correlation length, however, behaves inversely to the angular distribution: Therefore, the OPPC chains are better correlated than the tails of DMPC, with DLPC the least correlated. The values for ξ at an angle of 5° are 4.36 Å for DLPC, 4.79 Å for DMPC, and 5.30 Å for OPPC. Note that the data in the range between 35° and 55° are partly flawed by the missing data in the upper right corner of the RSM, as mentioned above.

ANALYSIS OF THE CHAIN CORRELATIONS: RADIAL DISTRIBUTION FUNCTION *G*(*R*)

In the previous section, we discussed the lateral chain ordering on the level of the chain correlation peak in reciprocal space. We have shown that the line shape of this peak is a Lorentzian and that the ϕ dependence of its intensity can be used as an empirical measure of the chain tilt distribution. We now leave the distribution of tilt angles aside, and in the following address the form of the radial distribution function $g(r)$ in 2D space. We start with the function $g(r, z)$ describing the 2D point field (fluid), which is generated by the intersection between the hydrocarbon chains and a plane at constant z in the hydrophobic region. Since each chain populates on average a cylindrical volume, we expect that the distribution function is approximately constant $g(r) = g(r, z)$ over the whole hydrophobic region. This assumption will be checked further below. If this is the case, $g(r)$ can also be identified with the 2D point field

TABLE 1 The fraction of the integrated scattering intensity $A(\phi)$ in the angular region $0° \leq \phi \leq 30°$, respectively $60° \leq \phi \leq 90°$

Angle region	0°–30°	60°–90°
OPPC	52.2%	19.3%
DMPC	49.1%	21.7%
DLPC	46.1%	23.7%

These values indicate an increasing flexibility of the chains with decreasing chain length.

obtained by the projection of the chain center of mass values onto the *x-y* plane. In short, a well-defined 2D liquid structure can be associated with the chains of each side of the bilayer. We further assume that the two sides are uncorrelated and follow the same statistics owing to the symmetry. Experimentally, $g(r)$ is probed in reciprocal space by a slice through the chain correlation peak at $\phi \simeq 0$.

The isotropic radial distribution function in 2D is defined as

$$g(r) = \frac{n(r, r+\Delta r)}{\rho \Delta V_{2D}}, \tag{3}$$

with $\Delta V_{2D} = 2\pi\, r\, \Delta r$ denoting the volume of a shell with inner radius r and outer radius $r+\Delta r (\Delta r \ll r)$, ρ the two-dimensional particle density, and $n(r, r + \Delta r)$ the number of atoms with a distance to the center atom in between r and $r + \Delta r$. Because of the isotropy, the radial distribution function can also be written as the Fourier-Bessel transform of the structure factor:

$$g(r) = \frac{1}{2\pi\rho}\int [S(q) - 1]\, J_0(qr) q\, dq. \tag{4}$$

Furthermore, we know experimentally that the structure factor has a Lorentzian lineshape, i.e.,

$$S(q) = I\frac{\omega^2}{(q - q_0)^2 + \omega^2} + y_0, \tag{5}$$

where I denotes the peak intensity, ω the HWHM, q_0 the center, and y_0 the baseline of the peak. To carry out the integral in Eq. 4, $S(q)$ is normalized by setting y_0 to 1. For this peak profile, it is possible to solve the integral exactly and write the radial distribution function in terms of Struve functions $\mathbf{H}_0(x)$ and Bessel functions $\mathbf{Y}_0(x)$ (Gradshteyn and Ryzhik, 2000; Abramowitz and Stegun, 1970)

$$g(r) = 1 + \frac{I\omega^2}{4\rho}\left[\frac{q_1}{q_1 - q_2}\{\mathbf{H}_0(-q_1 r) - \mathbf{Y}_0(-q_1 r)\} + \frac{q_2}{q_2 - q_1}\{\mathbf{H}_0(-q_2 r) - \mathbf{Y}_0(-q_2 r)\}\right], \tag{6}$$

using the complex parameters $q_{1/2} = q_0 \pm \mathrm{i}\,\omega$.

If the width of the peak is small compared to the peak center, $\omega/q_0 \ll 1$, $g(r)$ can be well approximated by

$$g(r) \simeq 1 + \frac{I\omega}{\rho}\sqrt{\frac{q_0}{2\pi}}\frac{e^{-\mathrm{r}/\xi}}{\sqrt{r}}\cos(q_0 r - \pi/4), \tag{7}$$

with $\xi = \omega^{-1}$ as the correlation length. (This approximate expression describes the chain ordering quite well. The next correction term is a factor of $\omega/2q_0$ smaller:

$$g(r) \simeq 1 + \frac{I\omega}{\rho}\sqrt{\frac{q_0}{2\pi}}\frac{e^{-r/\xi}}{\sqrt{r}}\left[\cos(q_0 r - \pi/4) + \frac{\omega}{2q_0}\cos(q_0 r + \pi/4) + O\left(\frac{\omega^2}{q_0^2}\right)\right]. \tag{8}$$

Thus it is the Lorentzian lineshape, which leads to the oscillatory behavior of the radial distribution function in the regime of medium and large r. In the regime of small r we expect a peak at a typical intramolecular bond length, and for even smaller r we expect $g(r) \simeq 0$ as known from fluid dynamics (Percus and Yevick, 1958; Verlet, 1967; Hansen and McDonald, 1986; Krause et al., 1988; Brunner et al., 2002).

From Eq. 7, one can determine the correlation length ξ from the exponential decay and, most importantly, the period $2\pi/q_0$ as well as the phase shift $\pi/4$ of the oscillatory term. The resulting chain-chain distance defined as the first maximum of $g(r)$ is calculated to the first order correction of the cosine

$$a \simeq \frac{9\pi}{4q_0} - \frac{3\omega}{2q_0^2}. \tag{9}$$

(For the parameters $q_0 = 1.39$ Å^{-1} and $\omega = 0.25$ Å^{-1}, this approximation gives $a \simeq 4.89$ Å; the maximum of the exact solution of the integral (Eq. 6) is located at $a = 4.86$ Å, a deviation of less than 1%.)

To verify these results, we have investigated the data of a published molecular dynamics simulation, which has been run on a bilayer with 200 POPC-molecules (Heller et al., 1993; see Fig. 1 *a*). We have first calculated the two-dimensional structure factor by Fourier transforming the atom coordinates and compared it to the experimentally evaluated reciprocal space mapping in Fig. 2. The Fourier transform of the MD data is shown in Fig. 4. The chain correlation peak at $q = 1.42$ Å^{-1} is clearly visible and is extended along a circle around the origin, in good agreement with the experimental results. An additional peak occurs at

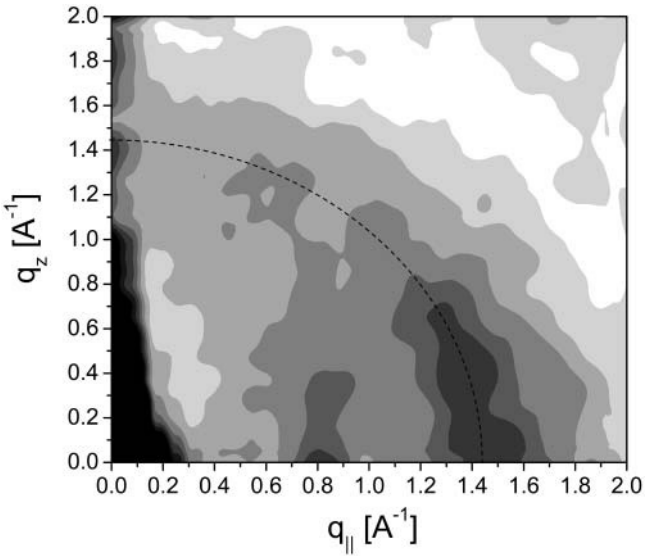

FIGURE 4 The 2D structure factor of an MD simulation of a bilayer of 200 POPC molecules (Heller et al., 1993), calculated by the Fourier transformation of the atomic coordinates and subsequent averaging in the *x-y* plane.

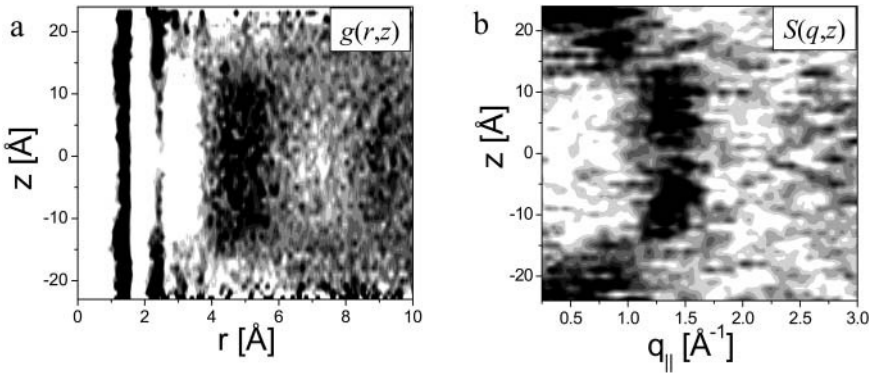

FIGURE 5 (*a*) Radial distribution function $g(r, z)$ and (*b*) structure factor $S(q, z)$ of the MD data set, computed for each slice in z. The region of the lipid chains ranges from $z = -12$ Å to $z = 12$ Å; the headgroups are located above and below, at $|z| > 12$ Å. The oscillation of $g(r)$ in the chain region is reflected by the chain correlation peak in $S(q)$ at $q = 1.39$ Å^{-1}. The peak in the structure factor at $q = 0.85$ Å^{-1} reflects the headgroup ordering; the two strong peaks in the radial distribution function at $r = 1.44$ Å and $r = 2.5$ Å are associated with intramolecular bond lengths.

$q_{\|} = 0.8$ Å^{-1}. This peak has been observed experimentally only in DMPC, in particular close to the main phase transition of the lipid, and can be attributed to short range ordering of the headgroups, as shown below. Note that the additional oscillatory pattern in Fig. 4 is due to finite size effects that arise from the numerical Fourier transformation.

To verify the theoretical form of $g(r)$, in particular the approximate form of Eq. 7, we first cut the simulated bilayer along the z axis in slices of the thickness 1 Å. From the atom coordinates in each slice, the radial distribution function and the structure factor have then been computed. Fig. 5 shows the resulting 2D plots for (*a*) $g(r, z)$ and (*b*) $S(q, z)$.

For small distances r, $g(r, z)$ is dominated by two strong peaks at $r = 1.44$ Å and $r = 2.5$ Å; the second one is mainly visible in the headgroup region (i.e., $|z| \geq 12$ Å). These features are attributed to intramolecular bond lengths. In the region of the chains ($|z| \leq 12$ Å), $g(r)$ exhibits an oscillatory behavior. Two broad maxima are observed at $r = 4.9$ Å and $r = 9.4$ Å. This regime of the radial distribution function describes the ordering of the chains in the membrane plane, corresponding to the chain correlation peak of the structure factor $S(q, z)$ at $q = 1.39$ Å^{-1}. (This value differs by 2% from the peak position obtained by 2D Fourier transform of the whole data set.) Furthermore, there is a peak located at $q = 0.85$ Å^{-1}, occurring only in the headgroup region. This feature has also been observed in the structure factor of the whole MD data, at small q_z (Fig. 4), as mentioned above. Hence we see that this peak must indeed be attributed to the correlated of the lipid headgroups.

Finally, we conclude the analysis by a check of consistency. To this end, the following operations are performed on the MD data. First, the structure factor $S(q, z)$ of the chains is computed by Fourier transformation of the atomic coordinates (Fig. 5), and then averaged in the range from $z = -12$ Å to $z = 12$ Å. Second, these data are fitted by a Lorentzian. Third, the fitting values are inserted in Eq. 7 and are compared to the radial distribution function that has been directly computed from the data, equally averaged in the range from $z = -12$ Å to $z = 12$ Å. The results of the first and second step are displayed in Fig. 6 *a*, with a least-squares fit (*solid line*) corresponding to $q_0 = 1.39$ Å^{-1}, $\omega = 0.25$ Å^{-1}, and $A = 1.16$. To plot Eq. 7, the 2D density of the chains is needed in addition. It was taken as $\rho = 0.031$ Å^{-2}, computed from the area per lipid of 65.5 Å^2, again according to the MD data (Heller et al., 1993). In Fig. 6 *b*, both procedures to compute $g(r)$ are compared. For $r \geq 4$ Å, the two curves agree quite well. We therefore conclude that the description of the chain liquid in terms of a 2D structure factor and 2D radial distribution function is consistent. Thus, the form of Eq. 7 should also describe the real bilayer reasonably well, given that the experimentally observed structure factor corresponds to a single Lorentzian peak.

SUMMARY AND DISCUSSION

We have shown that reciprocal space mappings are powerful tools to analyze the structure of lipid membranes. A direct comparison between the 2D scattering intensity distribution

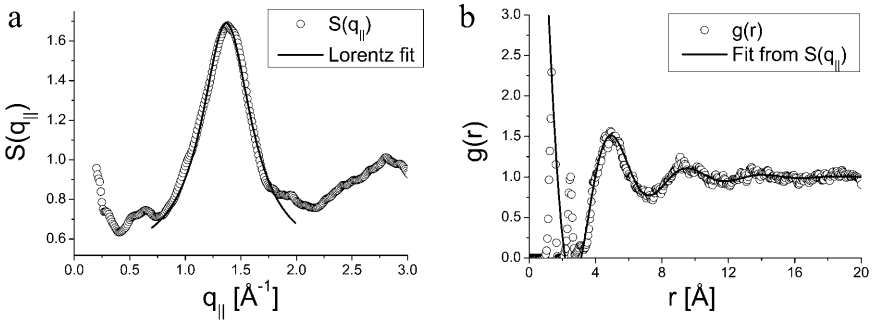

FIGURE 6 Structure factor and the radial distribution function of the lipid chains (averaged from $z = -12$ Å to $z = 12$ Å), both obtained from the MD data set: The parameters of the Lorentz fit (*solid*) of the chain correlation peak (*circles*) shown in *a* were used to calculate the approximate form of the radial distribution function by Eq. 7, shown in *b*. For $r > 4$ Å, the curve is found to agree very well with the one computed from the data.

and atomic MD coordinates can be performed by Fourier transformation. This approach helps to interpret scattering data, and conversely may be used to refine the starting configuration and parameters of a simulation. Furthermore, the comparative analysis of the scattering and MD data shows that at least to a certain extent the ordering of the hydrocarbon tails can be described by means of 2D liquid theory.

Using the theory of 2D liquids, we have derived an analytical expression for the 2D correlation function of the hydrocarbon chains fitting the MD data and the experimental structure factor. As a corollary, a relationship between the position of chain correlation peak q_0 and the interchain distance a, defined as the first maximum of $g(r)$, is obtained as $a = 9\pi/(4q_0)$. The radial distribution function (on an absolute scale) can be assessed experimentally, if either the number density is known, or if the scattering intensity was measured on an absolute scale. Unfortunately, the density or equivalently the area per lipid chain A_L cannot be extracted from the peak position without further assumptions. If, however, the MD simulation correctly describes the nature of the 2D hydrocarbon fluid state, one can generalize the relation between number density and peak position to the relationship $A_L \simeq 1.32(9\pi/4q_0)^2$. The assumption that the MD coordinates are reasonable is validated by the present comparison, in particular Figs. 2 and 4. Note that the deviation of the values of a between the MD and the experimental data of only 3% is not significant because q_0 and therefore a varies with temperature and humidity. However, the overall similarity between the curves computed from experiment and simulation suggests that the state of the lipid chains, notably the radial distribution functions, is well described by a two-dimensional fluid. With this knowledge at hand, observed changes in the peak position q_0 as a function of external fields (temperature, pressure, hydration, and chemical potentials) can then be converted into the important structural parameters interchain distance a and area per lipid chain A_L.

A second important result addresses the tilt of lipid chains. Although it has long been established that the lipid chains are dynamically disordered and partially tilted in the fluid state, x-ray diffraction of oriented membranes is highly sensitive to the lateral correlations of such tilted segments in adjacent chains. Owing to the high degree of orientation, the observed smearing of the chain correlation peak can exclusively be attributed to the tilted chains, rather than to the powder average of a mosaic sample. In other words, the data allow us to probe the distribution of chain tilting, rather than the distribution of membrane normal vectors.

In the future, the methodology presented here may be applied to lipid bilayers in varied external conditions, such as humidity, temperature, and chemical potentials, and eventually also electric fields. Furthermore, the addition of membrane-active molecules can be investigated by RSM of highly oriented bilayers. To this end, we note that it is possible to visualize the orientation of α-helical peptides adsorbed to or inserted in the bilayer (Münster et al., 2002) in an RSM. In a following paper, we will analyze RSM data of lipid/peptide model systems on the basis of atomic coordinates and Fourier transformation, in the same manner as the approach presented here on the chain correlation peak.

We thank the European Synchrotron Radiation Facility for providing beam time at the ID1 experimental station, and David Le Bolloch and Chenghao Li for help with the experiment.

Financial aid by the Deutsche Forschungsgemeinschaft through grants SA-772/3 and SA-772/4 is gratefully acknowledged.

REFERENCES

Abramowitz, M., and I. A. Stegun. 1970. Handbook of Mathematical Functions with Formulas, Graphs, and Mathematical Tables, 9th ed. Dover Publications, New York.

Ben-Shaul, A., I. Szleifer, and W. M. Gelbart. 1985. Chain organization and thermodynamics in micelles and bilayers. I. Theory. *J. Chem. Phys.* 83: 3597–3611.

Brunner, M., C. Bechinger, W. Strepp, V. Lobaskin, and H. H. von Grünberg. 2002. Density-dependent pair-interactions in 2D colloidal suspensions. *Europhys. Lett.* 58:926–932.

Dosch, H. 1992. Critical Phenomena at Surfaces and Interfaces. Springer Tracts in Modern Physics, Vol. 126. Springer-Verlag, Berlin and New York.

Feller, S. E. 2000. Molecular dynamics simulations of lipid bilayers. *Curr. Opin. Coll. Int. Sci.* 5:217–223 (and references therein).

Gradshteyn, I. S., and I. M. Ryzhik. 2000. Table of Integrals, Series, and Products, 6th ed. Academic Press, San Diego.

Hansen, J.-P., and I. R. McDonald. 1986. Theory of Simple Liquids, 2nd ed. Academic Press, New York.

Heller, H., M. Schaefer, and K. Schulten. 1993. Molecular dynamics simulation of a bilayer of 200 lipids in the gel and in the liquid-crystal phases. *J. Phys. Chem.* 97:8343–8360.

Helm, C. A., H. Möhwald, K. Kjaer, and J. Als-Nielsen. 1987. Phospholipid monolayer density distribution perpendicular to the water surface. A synchrotron X-ray reflection study. *Europhys. Lett.* 4: 697–703.

Katsaras, J. 1995. X-ray diffraction studies of oriented lipid bilayers. *Biochem. Cell Biol.* 73:209–218.

Koubi, L., M. Tarek, M. L. Klein, and D. Scharf. 2000. Distribution of halothane in a DPPC bilayer from MD calculations. *Biophys. J.* 78: 800–811.

Krause, R., G. Nägele, D. Karrer, J. Schneider, R. Klein, and R. Weber. 1988. Structure and self-diffusion in dilute suspensions of polystyrene spheres: experiment vs. computer simulation and theory. *Physika A.* 153:400–419.

Levine, Y. K., and M. H. F. Wilkins. 1971. Structure of oriented lipid bilayers. *Nature (Lond.).* 230:69–72.

Lindahl, E., and O. Edholm. 2000. Mesoscopic undulations and thickness fluctuations in lipid bilayers from molecular dynamics simulations. *Biophys. J.* 79:426–433.

Luzzati, V. 1968. X-ray diffraction studies of lipid-water systems. *In* Biological Membranes. D. Chapman, editor. Academic Press, New York. 71–124

Mashl, R. J., H. L. Scott, S. Subramaniam, and E. Jakobsson. 2001. Molecular simulation of dioleoylphosphatidylcholine lipid bilayers at differing levels of hydration. *Biophys. J.* 81:3005–3015.

Mennicke, U., and T. Salditt. 2002. Preparation of solid-supported lipid bilayers by spin-coating. *Langmuir.* 18:8172–8177.

Müller, J., C. Münster, and T. Salditt. 2000. Thermal denaturing of bacteriorhodopsin by x-ray scattering from oriented purple membranes. *Biophys. J.* 78:3208–3217.

Münster, C., J. Lu, B. Bechinger, and T. Salditt. 2000. Grazing incidence x-ray diffraction of highly aligned phospholipid membranes containing antimicrobial peptides magainin 2. *Eur. Biophys. J.* 28:683–688.

Münster, C., A. Spaar, B. Bechinger, and T. Salditt. 2002. Magainin 2 in phospholipid bilayers: peptide orientation and lipid chain ordering studied by x-ray diffraction. *Biochim. Biophys. Acta.* 1562:37–44.

Nagle, J. F., and J. Katsaras. 1999. Absence of a vestigial vapor pressure paradox. *Phys. Rev. E.* 61:7018–7024.

Nagle, J. F., and S. Tristram-Nagle. 2000. Structure and interactions of lipid bilayers: role of fluctuations. *In* Lipid Bilayers: Structure and Interactions. J. Katsaras and T. Gutberlet, editors. Springer, Berlin. 1–23.

Nagle, J. F., and M. C. Wiener. 1988. Structure of fully hydrated bilayer dispersions. *Biochim. Biophys. Acta.* 942:1–10.

Percus, J. K., and G. J. Yevick. 1958. Analysis of classical statistical mechanics by means of collective coordinates. *Phys. Rev.* 110:1–13.

Podgornik, R., and V. A. Parsegian. 1997. On a possible microscopic mechanism underlying the vapor pressure paradox. *Biophys. J.* 72:942–952.

Salditt, T. 2000. Structure and fluctuations of highly oriented phospholipid membranes. *Current Opinion in Colloid & Interface Science.* 5:19–26.

Salditt, T., T. H. Metzger, J. Peisl, and G. Goerigk. 1995. Nonspecular x-ray scattering from thin films and multilayers with the small-angle scattering equipment. *J. Phys. D.* 28:A236–239.

Salditt, T., C. Münster, Y. Lu, M. Vogel, W. Fenzl, and A. Souvorov. 1999. Specular and diffuse scattering of highly aligned phospholipid membranes. *Phys. Rev. E.* 60:7285.

Seelig, A., and J. Seelig. 1977. Effect of a single cis double bond on the structure of a phospholipid bilayer. *Biochemistry.* 16:45–50.

Seelig, J., and A. Seelig. 1980. Lipid conformation in model membranes and biological membranes. *Q. Rev. Biophys.* 13:19–61.

Seul, M., and M. J. Sammon. 1990. Preparation of surfactant multilayer films on solid substrates by deposition from organic solution. *Thin Solid Films.* 185:287–305.

Smith, G., E. B. Sirota, C. R. Safinya, and N. A. Clark. 1988. Structure of the L beta phases in a hydrated phosphatidylcholine multimembrane. *Phys. Rev. Lett.* 60:813–816.

Sun, W.-J., R. M. Suter, M. A. Knewtson, C. R. Worthington, S. Tristram-Nagle, R. Zhang, and J. F. Nagle. 1994. Order and disorder in fully hydrated unoriented bilayers of gel phase dipalmitoylphosphatidylcholine. *Phys. Rev. E.* 49:4665–4676.

Tieleman, D. P., and H. J. C. Berendsen. 1996. Molecular dynamics simulations of fully hydrated DPPC with different macroscopic boundary conditions and parameters. *J. Chem. Phys.* 105:4871–4880.

Verlet, L. 1967. Computer ''experiments'' on classical fluids. II. Equilibrium correlation Functions. *Phys. Rev.* 165:201–214.

Warren, B. E. 1933. X-ray diffraction in long chain liquids. *Phys. Rev.* 44:969–973.

White, S. H., and K. Hristova. 2000. Peptides in lipid bilayers: determination of location by absolute-scale x-ray refinement. *In* Lipid Bilayers: Structure and Interactions. J. Katsaras and T. Gutberlet, editors. Springer, Berlin. 189–203.

Wiener, M. C., and S. H. White. 1992. Structure of a fluid dioleoylphosphatidylcholine bilayer determined by joint refinement of x-ray and neutron diffraction data. III. Complete structure. *Biophys. J.* 61:437–447.

Yang, L., T. M. Weiss, T. A. Harroun, W. T. Heller, and H. W. Huang. 1999. Supramolecular structures of peptide assemblies in membranes by neutron off-plane scattering: method of analysis. *Biophys. J.* 77: 2648–2656.